Semigeostrophic Flow over Orography in a Stratified Rotating Atmosphere. Part I: Steady Three-Dimensional Solutions over Finite Ridges

WILLIAM BLUMEN AND BRIAN D. GROSS*

Department of Astrophysical, Planetary, and Atmospheric Sciences, University of Colorado, Boulder, CO 80309

(Manuscript received 27 February 1987, in final form 27 April 1987)

ABSTRACT

Three-dimensional, steady and inviscid flow over orography is examined by means of a semigeostrophic model. A constant Coriolis parameter f, uniform potential vorticity and a uniform basic flow characterize this model, first used by Merkine and Kálnay-Rivas. It is demonstrated that the neglect of ageostrophic accelerations, which characterize a semigeostrophic model, essentially requires low Rossby number flow Ro $\leqslant 0.3$, and relatively small values of the nondimensional mountain height $\epsilon/D \leqslant 0.5$, where $D \sim 3 \times 10^3$ m is the deformation depth. In this parameter range the disturbance potential is a solution of Laplace's equation; the atmosphere is semi-infinite and the finite-amplitude lower boundary is an isentropic surface.

The basic solution, expressed in prolate spheroidal coordinates, provides disturbance flows over an isolated mountain, finite ridges, and the limiting flow over a two-dimensional ridge. A comparison between the quasi-geostrophic and semigeostrophic responses to flow over the isolated mountain shows that (i) a rotational gradient wind correction to quasi-geostrophic flow that is independent of the basic current is introduced; (ii) the ageostrophic response associated with the basic current is an irrotational flow; and (iii) transformation of the semigeostrophic solution from geostrophic coordinate space to physical space displaces the circulation features on level surfaces radially outward from the vertical axis, and the displacement is proportional to the mountain height.

An anticyclonic bound vortex, representing the sum of the quasi-geostrophic solution and the rotational wind correction, occurs over an isolated circular mountain (mountain parameter $a = 0$) and over long ridges ($a > 0$). However, these circulations are not typically Taylor columns, since they are not two-dimensional: vertical motions occur for $0 < a < \infty$. The existence of a closed circulation when a basic current is considered is dependent upon Ro, ϵ/D and a. In general, relatively larger values of Ro (or smaller ϵ/D) inhibit the formation of a closed circulation, but there is slight dependence on a. In agreement with Merkine and Kálnay-Rivas, it is shown that a closed circulation will occur around a mountain at a larger value of Ro when the ridge line is aligned with the basic current than when the ridge line is normal to the current. The difference is relatively small, and probably unobservable in real flows.

A passive scalar disturbance is advected over ridges, characterized by different values of the mountain parameter a and orientation relative to the basic flow. This scalar field is advected anticyclonically around the tip of the ridge north of the current axis, but is retarded at the southern extremity of the ridge where the anticyclonic mountain circulation opposes the basic current. These features of frontal deformation are in qualitative agreement with synoptic analyses in geographic regions of orographic influence. Computed frontogenetical characteristics vary along selected trajectories. The distinctive features of frontogenesis are interpreted and compared with recent results obtained for flow over an infinite ridge.

1. Introduction

Flow interaction with orography has attracted considerable attention in atmospheric and oceanic sciences. This interest is related to observational evidence of orographic influences on a whole spectrum of fluid motions ranging from small-scale turbulence to planetary-scale phenomena. The present paper is concerned with stratified rotating flow over orographic features with a characteristic horizontal scale $L \geqslant 300$ km. Motions of this characteristic scale are associated with a Rossby number Ro $\leqslant 0.3$, and the flow dynamics may be examined within the context of semigeostrophic theory. Within the context of this theory, the advected momentum is approximated by geostrophic momentum, but the advecting velocity is not constrained by this approximation. The foundations of this theory have been carefully developed by Hoskins (1975).

The first use of semigeostrophic theory to examine flow over orography was presented by Robinson (1960), but restricted to flow in a vertical cross section: flow over a two-dimensional ridge. Merkine and Kálnay-Rivas (1976) extended the problem to flow over three-dimensional isolated mountains, examined the limitations of semigeostrophic theory, and compared some of their results to quasi-geostrophic solutions. Some recent work by Davies and Roth (1986) explores the progression of a front over three-dimensional orography, within the context of a semigeostrophic shallow-

* Center for Atmospheric Theory and Analysis, University of Colorado.

water model. In contrast to the extensive bibliography of quasi-geostrophic orographic flow problems that have attracted attention, application of semigeostrophic theory to orographic flow problems has been extremely limited.

The investigation by Merkine and Kálnay-Rivas, hereafter MK, represents a very important contribution to the literature, but apparently has received relatively little attention. This circumstance may be related to the fact that the authors' method of solution makes a detailed comparison between their results and those of the corresponding quasi-geostrophic analyses somewhat difficult to achieve, and the range of orographic features employed by MK is quite limited. Nonetheless, MK were able to extract some general properties of steady semigeostrophic flow over finite-amplitude orography that merit further investigation. The MK model is adopted in the present investigation, to achieve this purpose.

The use of geostrophic coordinates, and the neglect of some unimportant terms, provides not only mathematical simplicity but also achieves the desired comparison with the quasi-geostrophic formalism. The basic solution is expressed in prolate spheroidal coordinates, and flexibility is provided in the choice of boundary profiles. A limiting case is flow over an axisymmetric mountain with a circular planform. This mountain may also be elongated (resembling a prolate spheroid), and oriented in any direction relative to the basic flow: an infinite elongation provides a two-dimensional solution presented by Blumen and Gross (1986).

Within the context of the present model, it is shown that the closed circulation found by MK occurs when the magnitude of the quasi-geostrophic bound vortex exceeds the speed of the basic flow. Only the position of the closed circulation is affected by ageostrophic contributions contained in the semigeostrophic formulation. The conditions for a closed circulation to occur are derived as a function of the mountain height, Rossby number and a parameter a which provides the measure of the mountain elongation. The MK result, that a closed circulation will be more likely to occur when the finite ridge is aligned with the basic flow rather than normal to it, is also clarified. Some flow trajectories are displayed as a function of the mountain height and ridge elongation parameter a. Comparison with observed flow fields is achieved by an indirect approach. The steady solutions are used to advect a passive scalar disturbance, resembling a frontal configuration, past the various orographic features. The deformation of this frontal surface is compared with characteristics of observed frontal deformations by orography. The relatively close correspondence between the model produced results and the observed features leads to the speculative conclusion that the progression of a surface front past orography is primarily controlled by the mountain flow, not by the intrinsic frontal circulation.

The basic model is presented in section 2. Solutions are presented in section 3, and in section 4 the rotational and irrotational parts of the flow are displayed explicitly for the axisymmetric mountain case, in order to promote a comparison between semigeostrophic and quasi-geostrophic solutions. The bound vortex solution is explored in section 5. Trajectories of the total flow, and the deformations produced by the translation of a passive scalar past various orographic features, are presented both in planform and in vertical cross sections in section 6. Final remarks, concerning the applicability of the present results to real flow problems, appear in section 7.

2. Model

The steady state MK model, adopted here, is hydrostatic and inviscid; it is characterized by a constant Coriolis parameter f, a constant Brunt-Väisälä frequency N and a constant basic current $\bar{u}$, which flows over an isolated mountain or finite ridge $h(x, y)$. The geostrophic momentum approximation is employed and the potential vorticity q_g is uniform. All equations are put into nondimensional form, according to the scaling proposed by Pierrehumbert (1985), and transformed into geostrophic coordinate space using the transformation formulas of Hoskins (1975).

The so-called semigeostrophic system is represented by

$$\mathrm{Ro}u_a = -\mathrm{Ro}^2\left[(1+u_g)\frac{\partial v_g}{\partial X} + v_g\frac{\partial v_g}{\partial Y} + w\frac{\partial v_g}{\partial Z}\right], \tag{1}$$

$$\mathrm{Ro}v_a = \mathrm{Ro}^2\left[(1+u_g)\frac{\partial u_g}{\partial X} + v_g\frac{\partial u_g}{\partial Y} + w\frac{\partial u_g}{\partial Z}\right], \tag{2}$$

$$\mathrm{Ro}w = -\mathrm{Ro}^2\left[(1+u_g)\frac{\partial \theta}{\partial X} + v_g\frac{\partial \theta}{\partial Y}\right]\Big/\left(1+\frac{\partial \theta}{\partial Z}\right), \tag{3}$$

where the geostrophic velocities are

$$u_g = -\partial\Phi/\partial Y, \quad v_g = \partial\Phi/\partial X, \tag{4}$$

the potential temperature is

$$\bar{\theta}(Z) + \theta(X, Y, Z) = Z + \mathrm{Ro}\partial\Phi'/\partial Z, \tag{5}$$

and the potential Φ' is represented by

$$\Phi'(X, Y, Z) = -Y + \Phi(X, Y, Z). \tag{6}$$

The basic state is characterized by a constant static stability, $\partial\bar{\theta}/\partial Z = 1$, and a constant basic current, $\bar{u} = 1$.

The geostrophic coordinates (X, Y, Z) are defined by

$$X = x + \mathrm{Ro}v_g, \quad Y = y - \mathrm{Ro}u_g, \quad Z = z, \tag{7}$$

where (x, y, z) are physical space Cartesian coordinates directed, respectively, eastward, northward and vertically upward. The geostrophic velocities (u_g, v_g) and the ageostrophic velocities (u_a, v_a) are the (X, Y) com-

ponents of the flow, and the vertical velocity w is in the direction of Z. The Rossby number is defined as $\mathrm{Ro} = U/fL \leqslant 0.3$, where U represent the horizontal velocity scale and L is the characteristic scale of the orography, used to nondimensionalize the horizontal coordinates. The vertical coordinate is nondimensionalized by the deformation depth $D = fL/N$, and the scale of the vertical velocity is $UD/L \ll U$, with $D \sim 3 \times 10^3$ m and $L \geqslant 3 \times 10^5$ m. The disturbance potential temperature is scaled by $N^2 D\theta_0/g$, where θ_0 is a constant reference value and g denotes the acceleration of gravity.

The basic equation for the disturbance potential field Φ follows from the constraint of uniform potential vorticity $q_g = f\theta_0 N^2/g$, and is provided by Hoskins [1975, Eq. (25)] as

$$\mathrm{Ro}\left(\frac{\partial^2}{\partial X^2}+\frac{\partial^2}{\partial Y^2}+\frac{\partial^2}{\partial Z^2}\right)\Phi - \mathrm{Ro}^2\left[\frac{\partial^2\Phi}{\partial X^2}\frac{\partial^2\Phi}{\partial Y^2}-\left(\frac{\partial^2\Phi}{\partial X\partial Y}\right)^2\right]=0, \quad (8)$$

where the basic state is identically satisfied.

A semi-infinite atmosphere is specified with all variables required to decay to zero as $(|X|, |Y|, Z) \to \infty$.[1] The kinematic condition at the lower boundary is

$$w=\left[(1+u_g)\frac{\partial}{\partial X}+v_g\frac{\partial}{\partial Y}\right]h, \quad Z=h(x,y), \quad (9)$$

where the ageostrophic velocity components (u_a, v_a) are absorbed by the coordinate transformation (7). Substitution of (9) into (3) yields

$$\left[(1+u_g)\frac{\partial}{\partial X}+v_g\frac{\partial}{\partial Y}\right](Z+\theta)=0, \quad Z=h(x,y), \quad (10)$$

which may be satisfied by choosing the lower boundary to be an isentropic surface

$$Z+\theta=Z_0, \quad (11)$$

where Z_0 is the constant level approached as $(|X|, |Y|) \to \infty$.

Solutions of (8), that decay with distance and satisfy (11) provide the complete solution to this flow problem, since all variables in (1)–(6) are expressed in terms of Φ. This is a principal advantage of the semigeostrophic system, although the neglect of ageostrophic accelerations does provide a limitation.

3. Solutions

Merkine and Kálnay-Rivas solved the physical space version of (8) by a numerical approach. Here, the nonlinear terms in (8) will be neglected, although nonlinearity is retained through the coordinate transformation (7). Evaluation of the neglected terms is accomplished ex post facto in the Appendix using a solution of the three-dimensional Laplace's equation. It is shown that the neglected terms are relatively small provided that the ratio of the mountain height ϵ to the deformation depth D is constrained by $\epsilon/D \leqslant 0.5$. This is essentially the same constraint required to validate the geostrophic momentum approximations, also shown in the Appendix. Mountain heights ϵ are limited to about 2×10^3 m by the constraint $\epsilon/D \leqslant 0.5$, depending on the values of N and L used. Consequently, the neglect of the nonlinear terms in (8) is consistent with the geostrophic momentum approximation, and average orographic heights of most mountain chains are encompassed by the present model solutions.

Morse and Feshbach [1953, Eq. (10.3.47)] have provided a general solution of Laplace's equation as an infinite Fourier series in prolate spheroidal coordinates. The first term of this series will be used to represent $\mathrm{Ro}\Phi$; although limited, this truncated solution closely resembles the numerical solution of (8) presented by MK, and may be adapted to represent the response to isolated axisymmetric mountains and to long ridges. This solution is expressed as

$$\mathrm{Ro}\Phi=\mu^3\left(\frac{1+a}{a}\right)\ln\left(\frac{\xi+1}{\xi-1}\right)-\mu^3\ln[1+(a/2)^2], \quad (12)$$

where

$$\left.\begin{aligned}\xi&=(r_1+r_2)/a\\ r_1&=[X^2+Z^2+(Y+a/2)^2]^{1/2}\\ r_2&=[X^2+Z^2+(Y-a/2)^2]^{1/2}\end{aligned}\right\}, \quad (13)$$

μ^3 is a constant, and the parameter a represents a measure of the length to the breadth of the mountain.

The limit of (12) as $a \to 0$ is the source solution of Laplace's equation

$$\mathrm{Ro}\Phi=\mu^3/r, \quad (14)$$

where $r^2 = X^2 + Y^2 + Z^2$. The lower boundary is, from (11),

$$Z\left(1-\frac{\mu^3}{r^3}\right)=Z_0. \quad (15)$$

This boundary has a circular planform and, if $Z_0 = 0$, the mountain is a hemisphere of radius μ. (Note, however, that the vertical coordinate is scaled by $N/f \sim 10^2$.) The limit approached when $a \to \infty$ is

$$\mathrm{Ro}\Phi=-\mu^3\ln(X^2+Z^2)+\text{constant}, \quad (16)$$

which represents the potential for a source situated at the origin, $X = Z = 0$. With $\mu^3 = c^2/2$, the lower boundary is represented by

$$Z\left(1-\frac{c^2}{X^2+Z^2}\right)=Z_0, \quad (17)$$

[1] MK employ an upper-ridge lid boundary condition at $Z = H$, but this condition does not provide any qualitative differences in the results since all variables decay rapidly over the characteristic scale $Z \sim D < H$.

which has been used by Blumen and Gross (1986) to examine flow over an infinite ridge.

Consequently, the potential represented by (12) provides flow patterns over an isolated circular mountain ($a = 0$) and ridges of finite ($0 < a < \infty$) and infinite length ($a = \infty$). Moreover, the ridges may be oriented at different angles to the basic flow and, in particular, when the ridge line is parallel to $\bar{u}$, the coordinates (r_1, r_2) in (13) are replaced by

$$\left.\begin{aligned} r_1 &= [(X + a/2)^2 + Y^2 + Z^2]^{1/2} \\ r_2 &= [(X - a/2)^2 + Y^2 + Z^2]^{1/2} \end{aligned}\right\}. \tag{18}$$

4. Circular mountain solution

Physical aspects of the model are most clearly displayed by use of the source solution (14). Analysis of the flow over an infinite ridge has been presented by Blumen and Gross [1986, 1987], and flows over finite ridges are deferred to following sections.

Introduction of (14) into (1), (2) and (3), noting (4) and (6), yields the compact form

$$\mathrm{Ro}(\bar{u} + u_g + u_a) \approx \mathrm{Ro}\left[-\frac{\partial \phi}{\partial Y} + \frac{\partial}{\partial X}(\psi + \psi_w)\right], \tag{19a}$$

$$\mathrm{Ro}(v_g + v_a) \approx \mathrm{Ro}\left[\frac{\partial \phi}{\partial X} + \frac{\partial}{\partial Y}(\psi + \psi_w)\right], \tag{19b}$$

$$\mathrm{Ro}w \approx \mathrm{Ro}\frac{\partial \psi}{\partial Z}, \tag{19c}$$

where

$$\mathrm{Ro}\phi = -\mathrm{Ro}Y + \frac{\mu^3}{r} + \frac{\mu^6}{4r^4}, \tag{20a}$$

$$\mathrm{Ro}\psi = \mathrm{Ro}\mu^3 \frac{X}{r^3}, \tag{20b}$$

$$\mathrm{Ro}\psi_w = -\mathrm{Ro}\mu^6 \frac{9}{8}\frac{XZ^2}{r^8}, \tag{20c}$$

and $r^2 = X^2 + Y^2 + Z^2$. The variable $\mathrm{Ro}\phi$ represents the total streamfunction and $\mathrm{Ro}(\psi + \psi_w)$ the total velocity potential associated with the flow over the mountain represented by (15). Small terms associated with vertical advections in (1), (2) and (3) have been omitted, and the vertical advections themselves, represented by ψ_w in (19a, b), are much smaller than the remaining terms. Consequently, this term will be omitted from the present discussion, although all terms are retained in numerical evaluations of the solution.

The *quasi-geostrophic* solution is represented by the first two terms on the right-hand side of (20a), but in that case both Y and r are expressed in terms of *physical space coordinates* (x, y, z). The semigeostrophic contributions are provided by a rotational component $\mu^6/4r^2$, which represents a gradient wind correction to the geostrophic flow [e.g., Hoskins, 1975], and an irrotational component represented by (20b). However, all terms in (20a, b) are expressed in geostrophic coordinate space, so that there is also a horizontal displacement of each field according to (7).

The solutions will be examined at the lower boundary where the maximum velocities occur. The transformation to physical space, obtained from (4), (7), (14) and (15), is expressed by

$$x = (1 + \delta)X, \quad y = (1 + \delta)Y, \tag{21}$$

where $\delta = (z - z_0)/z$. The basic current also introduces a uniform y-coordinate displacement, as noted from (20a), but this contribution can be eliminated by a redefinition of the origin of coordinates. The physical space (x, y) coordinates are always stretched outward from the origin, relative to the geostrophic coordinates, because the geostrophic flow is an anticyclonic vortex. All differences between the quasi-geostrophic and semigeostrophic flows would be explained by this coordinate stretching if the ageostrophic velocities were not included in the semigeostrophic solution.

The relative importance of the ageostrophic terms is most clearly displayed in cylindrical coordinates:

$$\left.\begin{aligned} x &= R^* \cos\theta, \quad y = R^* \sin\theta \\ V_r &= v \sin\theta + u \cos\theta \\ V_\theta &= v \cos\theta - u \sin\theta \end{aligned}\right\}, \tag{22}$$

where (u, v) are velocities along (x, y) and (V_r, V_θ) are in the directions of (R^*, θ), and $V_\theta < 0$ for clockwise flow. The physical space representation of the velocity components in (19a), (19b) is given by

$$\begin{aligned} \mathrm{Ro}V_\theta &= \mathrm{Ro}(V_{\theta g} + V_{\theta a}) \\ &= -\frac{\delta}{1+\delta}R^* - \frac{\delta^2}{1+\delta}R^* - \mathrm{Ro}\delta \sin\theta, \end{aligned} \tag{23a}$$

$$\mathrm{Ro}V_r = \mathrm{Ro}\delta \cos\theta\left(1 - \frac{3R^{*2}}{R^{*2} + [(1+\delta)z]^2}\right), \tag{23b}$$

where (15) has been used to eliminate μ^3 and the constant translation has been omitted. The first term on the right-hand side of (23a) represents the geostrophic vortex $V_{\theta g}$, while the second term is the gradient wind correction. The remaining terms in (23a, b) represent the irrotational part of the flow.

The maximum values of δ and the corresponding values at the mountain half-width are displayed in Table 1. If, for example, the mountain scale is $L \approx 450 \times 10^3$ m and the velocity scale is $U \approx 15$ m s^{-1}, then $\mathrm{Ro} \approx 0.3$ and $\epsilon/D = \epsilon N/fL = 0.5$ corresponds to $\epsilon \approx 2.25 \times 10^3$ m. Under these circumstances the ratio of the gradient wind correction to the geostrophic wind, found from (23a), is $\delta = 0.273$ at the mountain half-width $R^* = 1$. The maximum value of the ageostrophic flow occurs at the mountain peak, where the velocity is $\mathrm{Ro}\delta$. As in the case of flow over an infinite ridge, the maximum occurs at the peak to preserve a constant

TABLE 1. Characteristic values of $\delta = (z - z_0)/z$ and z_0 corresponding to various nondimensional mountain heights ϵ/D. The values of z_0 are determined by evaluating (15) at the origin ($X = Y = 0$) and at the half-width, where the height is $\epsilon/2D$. Elimination of μ^3 produces an equation for $Z_0 = z_0$, which is solved by a numerical root finder.

ϵ/D	z_0	$\delta\|_{\text{origin}}$	$\delta\|_{\text{half-width}}$
0.1	1.167	0.079	0.041
0.2	1.035	0.162	0.088
0.3	0.907	0.249	0.142
0.4	0.785	0.338	0.203
0.5	0.667	0.428	0.273

mass flux over the mountain [Blumen and Gross, 1986]. The ratio $\gamma = \text{Ro}\nabla_H^2\psi/\text{Ro}\nabla_H^2\phi$, where $\nabla_H^2 = \partial^2/\partial X^2 + \partial^2/\partial Y^2$, provides a measure of the relative importance of the irrotational to rotational part of the flow. Use of (20a), (20b), and the transformations (21) and (22), produces

$$\gamma = \frac{3\,\text{Ro}R^*\cos\theta}{R^{*2}+[(1+\delta)z]^2}\left(\frac{4-5R^{*2}/\{R^*+[(1+\delta)z]^2\}}{2-3R^{*2}/\{R^*+[(1+\delta)z]^2\}}\right) \sim \frac{6\,\text{Ro}R^*\cos\theta}{R^{*2}+[(1+\delta)z]^2}. \quad (24)$$

Evaluation of (24) at the half-width of a mountain with a peak value $\epsilon/D = 0.5$ yields $\gamma \sim 2.5\,\text{Ro}(\cos\theta)$. On the other hand, the ratio of the irrotational velocity components to the rotational velocity is, by (23a, b), about the order of Ro at the half-width, but increases toward the peak. In any case, the advecting ageostrophic velocities, including the gradient wind correction, promote significant corrections to the geostrophic velocity field for values of $\text{Ro} > 0.1$. Yet the geostrophic momentum approximation is essentially valid for moderate values of the parameters, $\text{Ro} \leqslant 0.3$ and $\epsilon/D \leqslant 0.5$, as shown in the Appendix.

5. Mountain vortices and closed circulations

The steady solution, expressed by (12) and (1)–(6) is characterized by both a bound vortex and a flow forced by the basic current. MK have noted that the bound vortex is independent of the basic current, determined solely by ϵ/D and a in the present model. When $a = 0$, the circular vortex is represented explicitly by the first two terms on the right-hand side of (23a) expressed as $\text{Ro}V_\theta = -\delta R^*$. An extended discussion of this vortex solution, its relationship to the problem of the time-dependent evolution of the flow, and to the problem of flow blockage by the orography has been presented by MK. These latter problems cannot be approached by the present steady state model of flow over an isentropic lower boundary. The present approach represents an examination of the conditions for the existence of a closed steady state circulation as a function of the Rossby number Ro, the nondimensional mountain height ϵ/D and the mountain parameter a. This is the problem considered by MK, but the results obtained were limited.

The solution represented by (12) is used; (13) applies when the ridge line is normal to the basic current and (18) is applicable to flow parallel to the ridge line. In either case the condition that must be met for the occurrence of a closed circulation is

$$\text{Ro}(\bar{u}+u_g+u_a)=0, \quad X=0, \quad Y<0, \quad Z=h(0,Y). \quad (25)$$

Closed streamlines will occur when the magnitude of the anticyclonic vortex solution exceeds that of the basic current, directed along the x-axis. Condition (25) is applied on the boundary $Z = h(0, Y)$ because the vortex circulation decays with height. The availability of an analytic solution provides a clearer examination of condition (25), than that available from the numerical evaluations presented by MK, and a wider range of parameter values may be investigated.

Use of (12), (13), (1) and (4) yields, along $X = 0$,

$$\text{Ro}(\bar{u}+u_g) = \left[\text{Ro}+\mu^3\left(\frac{1+a}{a^2}\right)\left(\frac{2}{\xi^2-1}\right)\left(\frac{Y+a/2}{r_1}+\frac{Y-a/2}{r_2}\right)\right], \quad (26a)$$

$$\text{Ro}u_a = \text{Ro}(\bar{u}+u_g)\left[\mu^3\left(\frac{1+a}{a^2}\right)\left(\frac{2}{\xi^2-1}\right)\left(\frac{1}{r_1}+\frac{1}{r_2}\right)\right]. \quad (26b)$$

The term within square brackets in (26b) is positive for all parameter values. Consequently, the *occurrence* of a closed circulation is independent of the ageostrophic part of the flow, as shown by (25) and (26a, b). Evaluation of $\text{Ro}(\bar{u} + u_g) = 0$ on the boundary

$$Z\left[1-\mu^3\left(\frac{1+a}{a^2}\right)\left(\frac{2}{\xi^2-1}\right)\left(\frac{1}{r_1}+\frac{1}{r_2}\right)\right]=Z_0 \quad (27)$$

provides the condition,

$$\text{Ro}+\frac{Z-Z_0}{Z}\left[\frac{r_2(Y+a/2)+r_1(Y-a/2)}{r_1+r_2}\right]=0, \quad (28)$$

that must be met to realize a closed circulation around a ridge oriented normal to the basic current. An analogous result is obtained when the basic current is oriented along the ridge line. In this latter case (18) is used in the evaluation of (12) and (27) and, as above, condition (25) is independent of u_a. The condition for a closed circulation on the mountain reduces to

$$\text{Ro}+\frac{Z-Z_0}{Z}Y=0. \quad (29)$$

The coordinate Y appearing in (28) and (29) is related to Z through (27), and the location in physical space is found from (7).

The case $a = 0$ reduces (28) to (29) with the mountain shape provided by (15). A closed circulation will occur at ground level, for a given mountain height ϵ/D, if Ro is less than or equal to the values displayed in Table 2. Larger values of Ro, equivalently the strength of the basic current, will prevent the occurrence of a closed circulation. Typical examples of each situation are displayed by MK (Figs. 6 and 7). The parameters associated with the circulation displayed in the figures in MK are appropriate for the critical conditions provided in Table 2.

The corresponding conditions for a closed circulation to occur when $a \neq 0$ are presented in Fig. 1 for ridge heights $\epsilon/D = 0.3$ and $\epsilon/D = 0.5$. The range of Rossby numbers between the solid and dashed lines, for each case, represents the region in parameter space in which a closed circulation will occur around a ridge that is oriented along the basic flow but not around a ridge placed normal to the basic flow. These results agree qualitatively with those presented by MK (Figs. 7 and 8), but there is a difference in the value of Ro that provides the separation between closed and open circulations. This difference is most likely related to the neglect of the nonlinear terms in (8), which are relatively insignificant when $\epsilon/D \leqslant 0.5$. However, the nondimensional height used by MK, when $a \neq 0$, corresponds to $\epsilon/D = 0.9$. The increase in the magnitude of the peak vortex speed with a is presented in Fig. 2. This increase is relatively small, and the difference in the peak speeds corresponding to the two different ridge orientations also remains small.

The present results do confirm the fact, pointed out by MK, that a closed circulation will occur around a ridge oriented with the basic flow more readily than around a ridge normal to the flow. However, the difference between the characteristic values of Ro associated with each circulation is small, as revealed in Fig. 1, and the simplicity of the model would indicate that verification of this circulation feature under atmospheric conditions would be highly unlikely.

The limiting value of $u_g(0, Y, Z)$ associated with the case represented by (29) is

$$\mathrm{Ro}u_g \to \frac{2\mu^3 Y}{X^2 + Y^2}, \quad a \to \infty. \tag{30}$$

Elimination of μ^3 by means of (17) recovers the value appearing in (29). As expected the velocity increases from the value associated with a circular mountain ($a = 0$) to that associated with an infinite ridge. The position of the maximum remains approximately at the position of the mountain half-width ($Y = 1$) in geostrophic coordinate space, as shown in Fig. 2. The values of $u_g(0, Y, Z)$ associated with (26a) must be determined by numerical evaluations of u_g as a function of a. The maxima appearing in Fig. 2 have essentially reached a limiting value when $a = 12$. The peak value of u_g associated with $|Y| \approx a/2$, and

$$|u_g| \approx \mu^3/Z, \quad a \to \infty \tag{31}$$

where Z is evaluated essentially at the level of the mountain half-width.

It is tempting to refer to the closed circulations described for the present model as Taylor columns or as Taylor cones. However, the bound vortex associated with (12) is *not* a two-dimensional circulation when $a \neq 0$. Evaluation of (3) by the source solution (14), corresponding to $a = 0$, confirms that Row = 0: the circular vortex solution is two-dimensional. Evaluation of Row by means of (12) and (13) is displayed in Fig. 3 for $a = 4$ and $a = 12$, with $\epsilon/D = 0.5$.

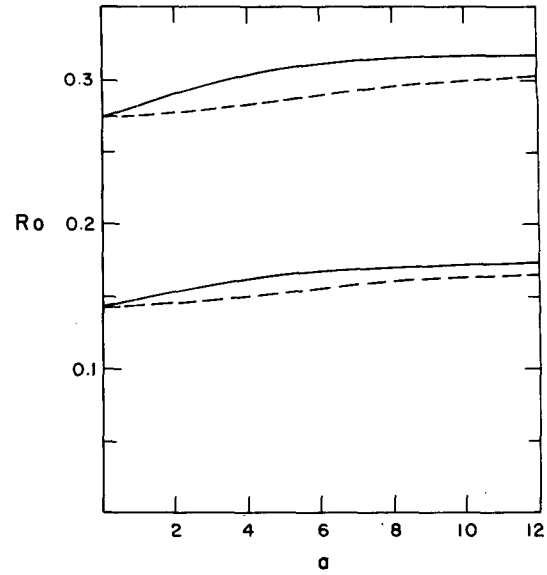

FIG. 1. Critical Rossby numbers, associated with a closed circulation, as functions of the mountain parameter a ($a = 4$ corresponds to a length to width ratio of the ridge equal to 2; $a = 12$ corresponds to 5). The upper two curves are associated with $\epsilon/D = 0.5$, the lower curves with $\epsilon/D = 0.3$. The solid curves apply to a ridge line parallel to the basic flow, and the dashed curves apply to a ridge aligned normal to the basic flow.

TABLE 2. Relationship between nondimensional mountain height ϵ/D, associated with (15), and Rossby number Ro that provide the condition for a closed circulation to occur. The mountain parameter is $a = 0$.

ϵ/D	0.1	0.2	0.3	0.4	0.5
Ro	0.04	0.09	0.14	0.20	0.27

6. Passive scalar transport over mountains

Oceanic observations have provided quite convincing evidence that the type of circulations produced in the present model do occur over sea mounts, e.g.,

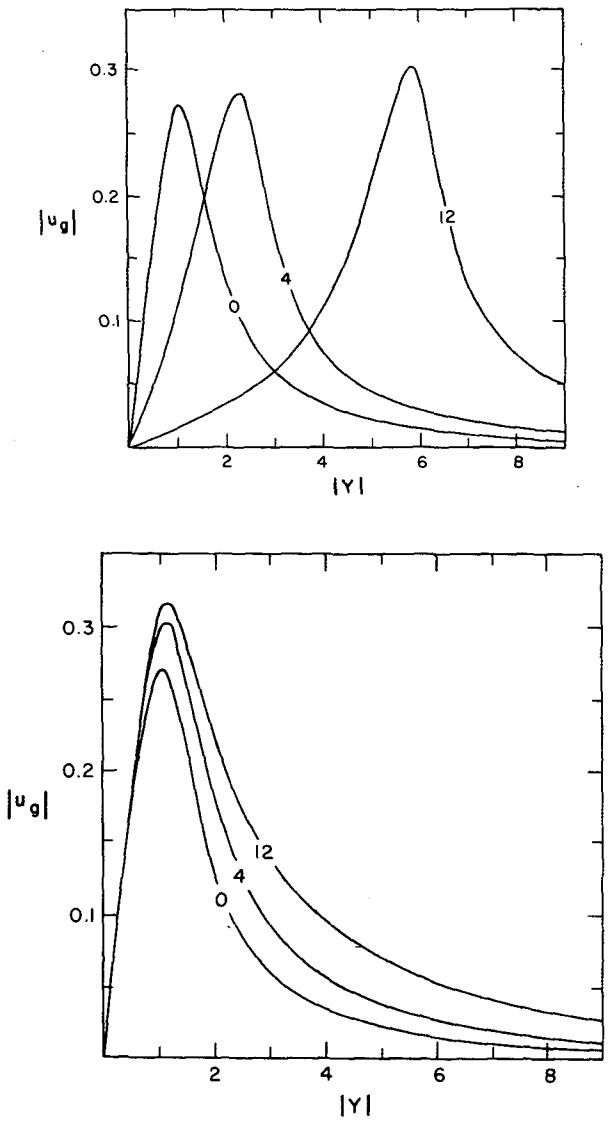

FIG. 2. Geostrophic velocities u_g, represented by (26a), along the Y-axis at ground level. The mountain parameters are $a = 0$ (circular planform), $a = 4$ (length to width ratio equal to 2), and $a = 12$ (length to width ratio equal to 5). The upper panel is associated with a ridge aligned normal to the basic flow, and the lower panel applies to a ridge aligned with the basic flow. The peak values are equal to the Rossby numbers displayed in Fig. 1 for $\epsilon/D = 0.5$.

Meinke (1971), Owens and Hogg (1980), and Gould, Hendry, and Huppert (1981). The observations presented by these authors show that bottom-trapped eddies are anticyclonic and decay over a Rossby depth. Further, the largest velocities occur where the basic current complements the eddy circulation and, in accord with theory, relatively strong current speeds inhibit the formation of closed circulations.

There does not appear to be the same type of observational evidence to support a close association with these model circulations and atmospheric circulations over isolated mountains. Among the various features that have not been considered and which may be very important are (i) nonisentropic lower boundaries, (ii) basic flow velocity shears (horizontal and vertical), (iii) nonuniform static stability and potential vorticity, and (iv) secondary circulations, such as those associated with fronts, that interact with the mountain circulation. However, an attempt will be made to verify the qualitative circulation features of the present model by means of an indirect approach.

Many observations are available of frontal progression over orography, and the particular signatures of such interactions are represented in Fig. 4, which has been reproduced from Smith (1986). This figure displays a synthesis of front and mountain interactions for various orientations of a front as it intersects a relatively long ridge. Such an interaction cannot be replicated by the present model, yet it is possible to examine a limiting situation. The present approach does not take into account the frontal circulation; the front is treated as a passive scalar disturbance, and is advected over orography in order to compare the frontal distortion in these simulations with those in Fig. 4. Incorporation of frontal dynamics requires the use of a more realistic, and a necessarily more complex, model to clarify the physical processes that are important in frontal interactions with orography. This preliminary step only provides an examination of some characteristic translational properties of the mountain circulation as functions of the mountain shape and its orientation relative to the approaching front.

The ground-level passage of two material surfaces over mountains with different aspect ratios and orientations relative to the basic flow are displayed in Fig. 5. Trajectories were calculated by integrating $(\dot{X}, \dot{Y}) = (u_g, v_g)$ and transforming coordinates to physical space by means of (7). The two salient features in this figure are the spatial deformation and the change in the separation of these material surfaces.

The spatial deformation is due primarily to advection by the mountain circulation: the scalar field is accelerated where the basic flow is enhanced by the anticyclonic mountain circulation and retarded where the basic flow is opposed by the mountain circulation. In Figs. 5(a–c), the cross-stream scale of the deformation tends to decrease as the parameter a increases. Figure 2 shows that the *magnitudes* of the cross-ridge velocities at the northern and southern ends of the mountain are relatively insensitive to the parameter a, hence the characteristic cross-stream horizontal shear of the mountain circulation and the associated deformation decrease as this parameter increases. However, as the ridge line becomes more aligned with the basic flow, the material surfaces are under the influence of the mountain circulation for a longer period of time. The material surfaces become progressively more deformed until they are nearly parallel to the basic flow, as depicted in Figs. 5(d, e). The critical Rossby number

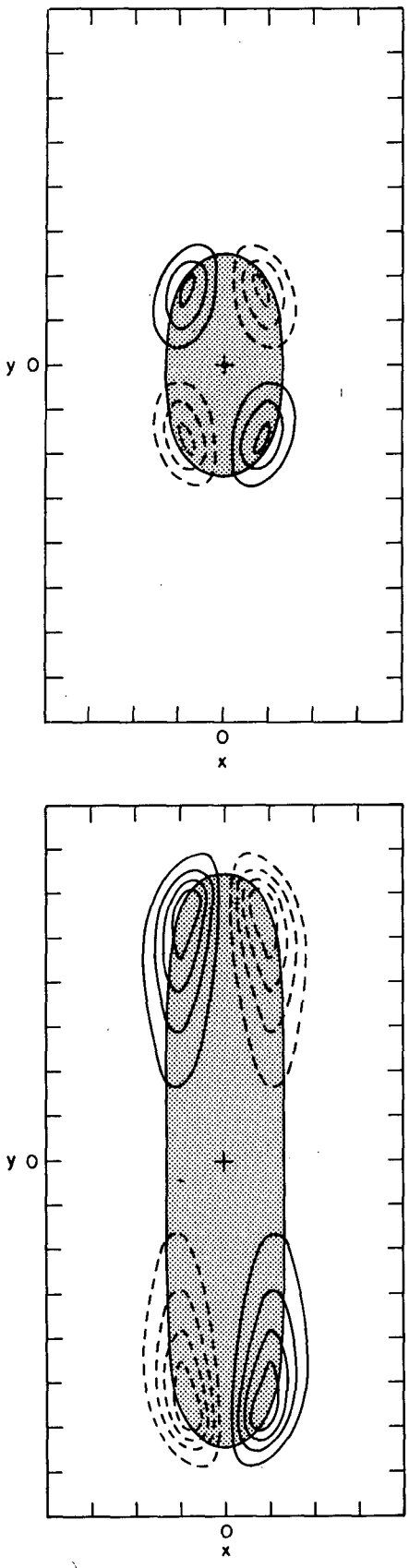

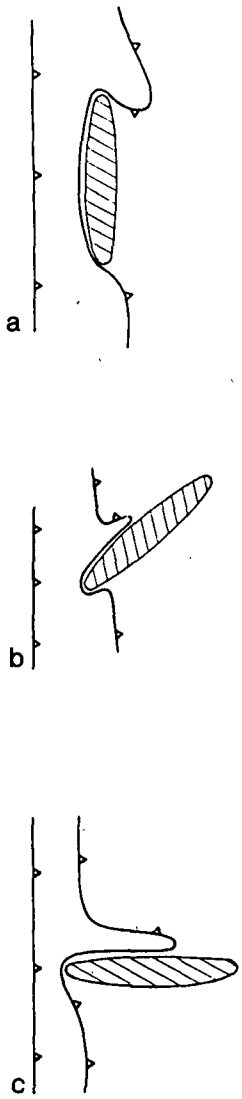

FIG. 4. Three common geographical configurations for a cold front distorted by a mountain, according to Smith (1986).

R_c, that would produce stagnation is not attained in the circulations presented in Fig. 5. However, the flow is closer to stagnation in Fig. 5(e), so that the combination of the ridge alignment and the reduced flow speed create the largest deformation of the material surfaces.

The three deformation patterns in Figs. 5(c–e) agree qualitatively with Smith's (1986) synthesis of the observed patterns shown in Fig. 4. The present model cannot reproduce the observed blocking by the moun-

FIG. 3. Vertical velocities w at ground level associated with the bound vortex solution, and nondimensional mountain height $\epsilon/D = 0.5$. The solid lines represent $w > 0$; the dashed lines are $w < 0$. The contour interval is 5×10^{-3} m s^{-1}; $|w|_{max} = 1.6$ cm s^{-1} in upper panel ($a = 4$) and $|w|_{max} = 2.5$ cm s^{-1} in the lower panel ($a = 12$).

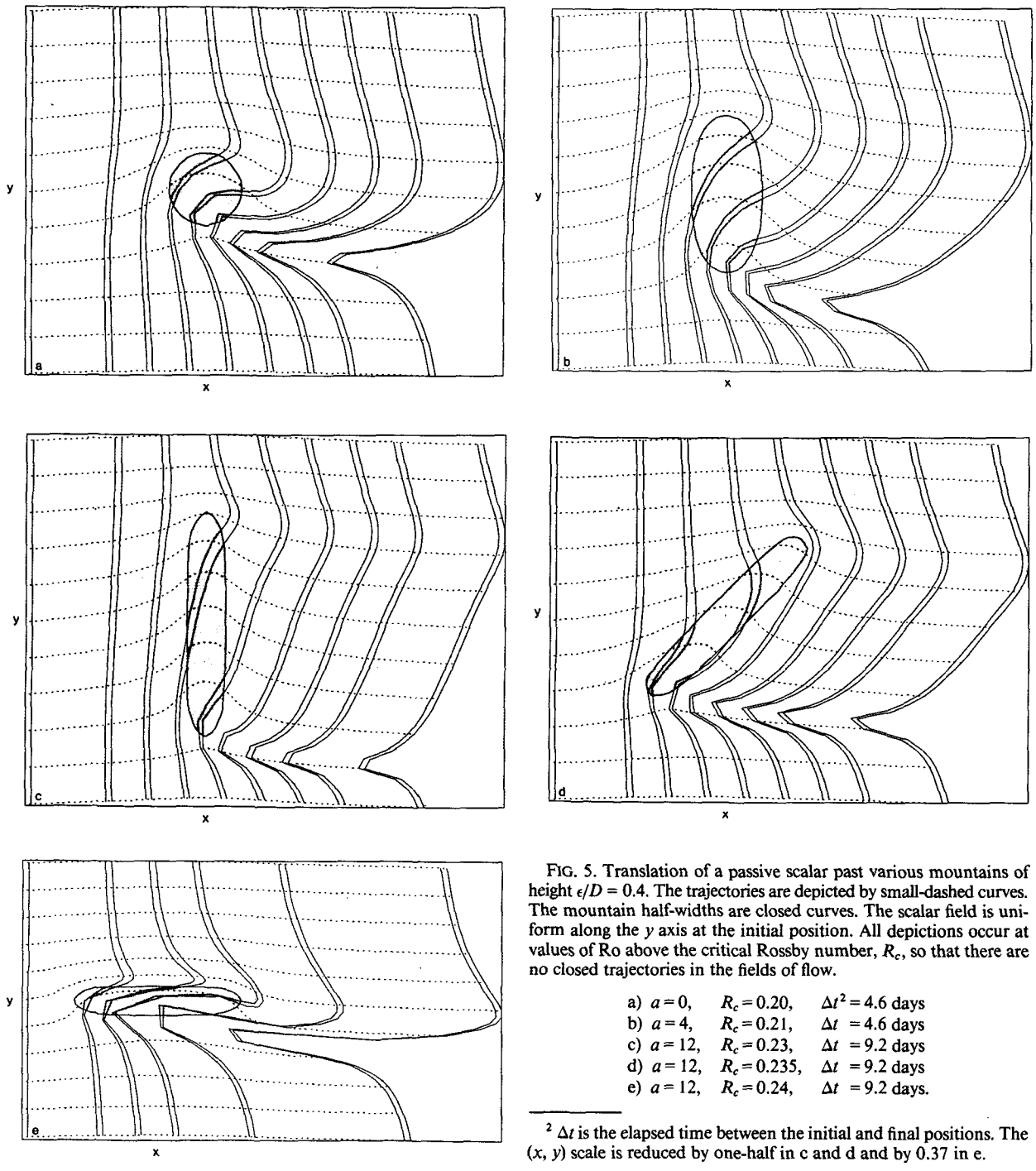

FIG. 5. Translation of a passive scalar past various mountains of height $\epsilon/D = 0.4$. The trajectories are depicted by small-dashed curves. The mountain half-widths are closed curves. The scalar field is uniform along the y axis at the initial position. All depictions occur at values of Ro above the critical Rossby number, R_c, so that there are no closed trajectories in the fields of flow.

a) $a = 0$, $R_c = 0.20$, $\Delta t^2 = 4.6$ days
b) $a = 4$, $R_c = 0.21$, $\Delta t = 4.6$ days
c) $a = 12$, $R_c = 0.23$, $\Delta t = 9.2$ days
d) $a = 12$, $R_c = 0.235$, $\Delta t = 9.2$ days
e) $a = 12$, $R_c = 0.24$, $\Delta t = 9.2$ days.

[2] Δt is the elapsed time between the initial and final positions. The (x, y) scale is reduced by one-half in c and d and by 0.37 in e.

tain. In a complementary investigation, Smith (1982) displayed deformation patterns similar to those in Fig. 5, but attention was restricted to large Rossby numbers, $\mathrm{Ro} \gtrsim 1$. We may speculate that the passage of a passive scalar over orography is controlled primarily by the mountain circulation.

The rate of separation of frontal surfaces is associated with frontogenesis and frontolysis. For convenience this nomenclature may be adopted in the description of the confluence and difluence of material surfaces. Consider the advection of a passive scalar G satisfying $\dot{G} = 0$. The change in the gradient of G is

$$\frac{d}{dt}\left(\frac{\partial G}{\partial s}\right) = -\frac{\partial \dot{s}}{\partial s}\frac{\partial G}{\partial s} - \frac{\partial w}{\partial s}\frac{\partial G}{\partial z}, \tag{32}$$

where s is the distance and $\dot{s}$ is the horizontal velocity along a trajectory. The first term on the right-hand side of (32) corresponds to horizontal convergence and the second to vertical tilting. These forcing terms have been calculated at the points indicated by dots in Fig. 6, along the three trajectories, at the upstream and downstream half-height of the mountain. The results are presented in Table 3. These numbers should not be interpreted as indicative of realistic magnitudes of frontogenetical/frontolytical forcing because in the present model the passive scalar gradients may be chosen arbitrarily.

The horizontal convergence is antisymmetric about the ridge line along all three trajectories, which agrees with the two-dimensional results of Blumen and Gross (1987). The tilting term is large in the three-dimensional solution as a consequence of the initial tilt imposed on the material surfaces. Along trajectory a, the magnitude of the tilting term is larger than the magnitude of the convergence term. This feature is related to the vertical velocity field of the mountain circulation shown in Fig. 3: the vertical velocity induced by uniform cross-ridge flow across the northern end of the mountain is enhanced. As a consequence, the tilting term and convergence term are both frontolytical at the upstream position in Fig. 6, while at the downstream position net frontolysis results from the dominant frontolytical tilting term. Along trajectory b, the convergence is weak because the horizontal velocity gradients are small at the mountain half-width. The tilting is only slightly weaker than along trajectory a: the vertical velocity associated with the mountain circulation is small near the middle of the ridge, but the vertical velocity associated with the basic flow is largest there. This produces net frontolysis upstream and downstream. Along trajectory c, the tilting is weak because the vertical velocity field due to the mountain circulation counteracts the vertical velocity field produced by the cross-ridge uniform flow. Yet, large convergence may be associated with the deceleration induced by the horizontal mountain circulation opposing the uniform cross-ridge flow. The result is net frontolysis at the upstream point and net frontogenesis at the downstream point.

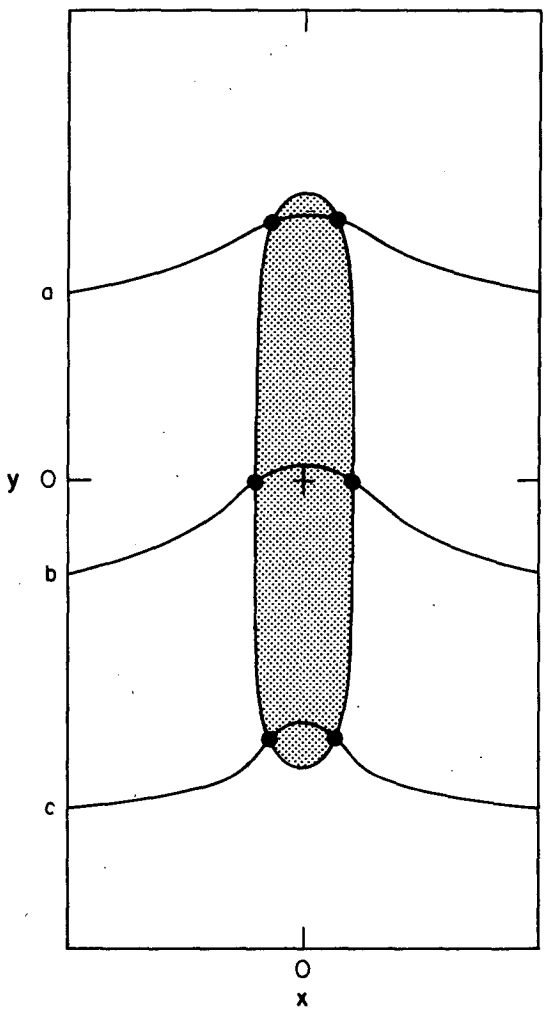

FIG. 6. Selected trajectories for computation of the frontogenetical forcing terms described in the text. The dots locate the points associated with the values in Table 3. $a = 12$ and $\epsilon/D = 0.4$.

The distortion of material surfaces by the mountain circulation is confined to within a Rossby depth of the ground $z \sim D$, in agreement with the oceanic observations. This feature is evident in the vertical cross sections displayed in Fig. 7(a–c) that show the passage of two material surfaces along the three trajectories (a–c) in Fig. 6. It is evident that the frontogenetical features exhibited along these trajectories are not entirely characterized by the measures presented in Table 3. The presentation in Fig. 7 serves to illustrate that the characteristic circulations around mountains could be expected to provide diverse frontogenetical features that will vary from point to point. However, this speculation is limited by the absence of characteristic frontal circulations.

7. Final remarks

The analytic solution (12) of the model equations provides a relatively simple tool to examine the numerical solutions presented by MK, and to expose some basic properties of the motion. This solution (12) has the desirable quality that it describes flow over an isolated mountain as one limit and flow over an infinite ridge in the other extreme, thus providing a unified treatment of both two- and three-dimensional steady flows over orography. However, it is not possible to completely shake off three-dimensional features of the orographic disturbance. Although the flow does tend to become two-dimensional in the central portions of a long ridge aligned normal to the basic flow, the flow

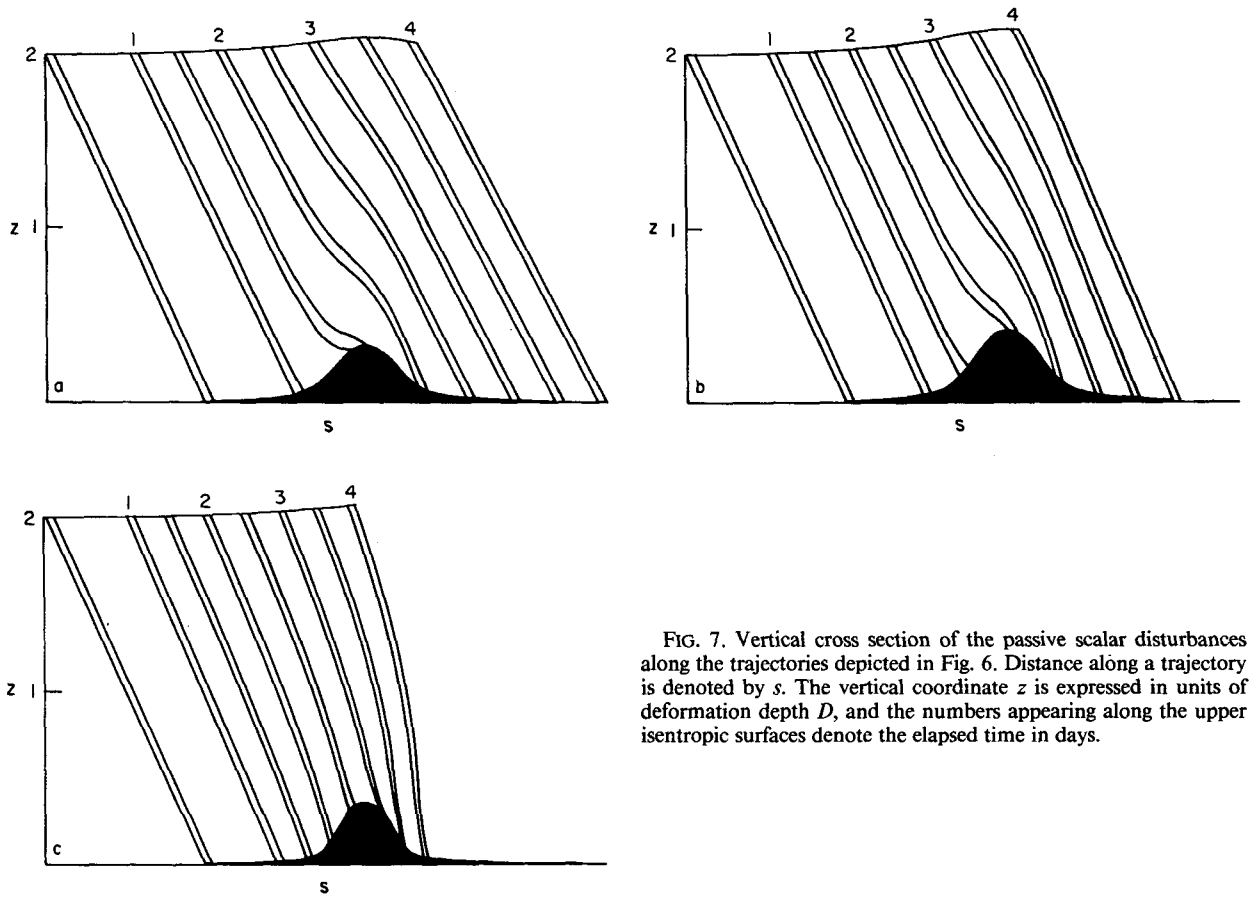

FIG. 7. Vertical cross section of the passive scalar disturbances along the trajectories depicted in Fig. 6. Distance along a trajectory is denoted by s. The vertical coordinate z is expressed in units of deformation depth D, and the numbers appearing along the upper isentropic surfaces denote the elapsed time in days.

is decidedly three-dimensional near the extremities. These are the regions where the interplay between the strength of basic flow, as measured by the Rossby number, and the strength of the anticyclonic mountain vortex, as measured by the nondimensional height ϵ/D, is most prominent. Further this interplay is relatively insensitive to the mountain parameter a, since the strength of the mountain vortex is relatively insensitive to a. Consequently, closed circulations may occur over long ridges about as readily as over an isolated mountain in parameter ranges that characterize real flows $\mathrm{Ro} \leqslant 0.3$ and $\epsilon/D \leqslant 0.5$.

TABLE 3. Values of the forcing terms at the points indicated in Fig. 6. The upstream and downstream points are at the half-height of the ridge. The absolute values are arbitrary because the passive scalar gradients are arbitrarily chosen. Positive values indicate a tendency for the material surfaces to decrease their separation, i.e., frontogenesis.

		Horizontal convergence	Vertical tilting
a	upstream	−1.382	−2.405
	downstream	1.317	−3.417
b	upstream	−0.5824	−2.153
	downstream	0.6234	−2.262
c	upstream	−1.537	−1.098
	downstream	1.482	−1.152

It has also been shown that the characteristic circulations associated with the various mountains considered, and this orientation relative to the basic flow produce distortions of a passive scalar field that are not unlike characteristic distortions of cold fronts that encounter mountain barriers. An interesting problem posed by this result concerns evaluation of the relative importance of the secondary direct circulation that tends to maintain thermal wind balance in the presence of disruptive frontogenetical processes. Perhaps this interaction between the frontal and mountain circulations is exhibited in windward blocking of the front and/or in the physical processes that promote leeside cyclogenesis? These questions cannot be answered by means of the present model results. However, it has been possible to clarify the role of the basic flow and the mountain vortex, and to evaluate the relative magnitude of the irrotational part of the disturbance, compared to the rotational component, in characteristic orographic flows constrained by the geostrophic momentum approximation. The role of nonisentropic

boundaries, the time evolution of the flow and, particularly, the possible occurrence of instabilities of shearing flows are future concerns.

Some properties of the motion that do not appear to be relevant to atmospheric flows, or at least are not observable, are 1) the existence of a *three-dimensional,* steady, bound vortex over elongated obstacles ($a \neq 0$), and 2) the existence of a relatively small range of Rossby numbers in which a closed mountain circulation can appear over a ridge aligned with the basic flow but not over a ridge that is aligned to the basic flow. It is possible that these phenomena could be replicated in a laboratory model, but the presence of an Ekman boundary layer could change the character of the motion in precisely the region where these features are most prominent. The relative importance of these phenomena under oceanic and atmospheric conditions cannot be evaluated at this time.

Acknowledgments. Financial support for this investigation was provided by the National Science Foundation under NSF Grants ATM 84-18625 and ATM 86-17636. The numerical computations were carried out on the Pyramid 90X super minicomputer at the University of Colorado Center for Atmospheric Theory and Analysis. We thank Professor R. B. Smith for permission to reproduce Fig. 4. William Blumen expresses his appreciation to the faculty and staff of the Naval Postgraduate School for their hospitality during 1986 when this study was initiated.

APPENDIX

Evaluation of Neglected Terms in the Model

1. The quadratic terms in (8).

The neglected terms will be evaluated with the axisymmetric solution (14), satisfying the lower boundary condition (15). This solution is associated with the largest curvature of the flow, and should provide a stringent bound on the relative magnitude of the neglected terms in (8).

First the constant μ^3 in (15) is determined by setting $Z - Z_0 = \epsilon/D$ at $X = Y = 0$, where ϵ/D represents the nondimensional mountain height. The value of μ^3 is

$$\mu^3 = (\epsilon/D)(Z_0 + \epsilon/D)^2. \tag{A1}$$

Substitution of (14) into (8), and use of (15), yields

TABLE 4. Ratio of the two terms in (A2) at the origin ($X = Y = 0$, $Z - Z_0 = \epsilon/D$). This ratio is smaller at lower elevations, $Z - Z_0 < \epsilon/D$, along the boundary.

ϵ/D	0.1	0.2	0.3	0.4	0.5	0.6
Ratio	0.04	0.08	0.12	0.17	0.21	0.26

TABLE 5. Evaluations of the ageostrophic and Coriolis accelerations, defined in (A4). The evaluations were carried out along the $X = 0$ axis for $Y \geq 0$ and along the $Y = 0$ axis for $X \geq 0$. The parameters are Ro = 0.3, $\epsilon/D = 0.5$ and $Z_0 = 0.667$. The results are presented in height above the reference level Z_0, which are irregularly spaced locations along the (X,Y) axes.

	$X = 0$		$Y = 0$	
$Z - Z_0$	$\mathrm{Ro}^3 D^2 u_g$	$\mathrm{Ro}(1 + u_g + u_a)$	$\mathrm{Ro}^3 D^2 v_g$	$\mathrm{Ro}(v_g + v_a)$
0.10	−0.052	0.569	−0.002	−0.229
0.20	−0.182	0.694	−0.080	−0.325
0.30	−0.210	0.746	−0.241	−0.353
0.40	−0.195	0.718	−0.175	−0.305
0.45	−0.153	0.655	−0.124	−0.244
0.50	−0.055	0.429	—	0

$$\frac{Z - Z_0}{Z}\left[1 - 3Z^2\mu^{-2}\left(\frac{Z - Z_0}{Z}\right)^{2/3}\right] + \left(\frac{Z - Z_0}{Z}\right)^2\left[2 - 3Z^2\mu^{-2}\left(\frac{Z - Z_0}{Z}\right)^{2/3}\right] = -\partial^2\Phi/\partial Z^2, \tag{A2}$$

where μ is defined by (A1). The first term on the left-hand side of (A2) represents the relative vorticity $\nabla_H^2\Phi$ in geostrophic coordinate space; the second term represents the evaluation of the quadratic term in (8). The ratio of these terms is the order of $\delta = (Z - Z_0)/Z = (z - z_0)/z$.

However, a more accurate evaluation of this ratio provides the maxima presented in Table 4. Neglect of the quadratic terms in (8) appears to be warranted if $\epsilon/D \leq 0.5$.

2. The ageostrophic accelerations

The ageostrophic velocities (u_a, v_a) are defined in (1) and (2). Validity of the geostrophic momentum approximation requires, according to Hoskins (1975), that the acceleration of these quantities be small in comparison with the Coriolis accelerations that appear in the same component equation of motion. The present evaluation considers the solution associated with (14), and evaluation is on the boundary. Introduction of the notation

$$D \equiv (1 + u_g)\frac{\partial}{\partial X} + v_g\frac{\partial}{\partial Y} + w\frac{\partial}{\partial Z} \tag{A3}$$

and use of (1) and (2) yields the conditions that constrain the geostrophic momentum approximation

$$\left.\begin{aligned} \mathrm{Ro}^3 D^2 u_g &\ll \mathrm{Ro}(1 + u_g + u_a) \\ \mathrm{Ro}^3 D^2 v_g &\ll \mathrm{Ro}(v_g + v_a) \end{aligned}\right\}. \tag{A4}$$

Evaluations of the terms in (A4) are presented in Table 5. These results are in essential agreement with those

presented by MK. There are limited regions along the boundary where the omitted accelerations are not negligible, particularly near the mountain peak. It is here where the ageostrophic accelerations are most prominent. However, at lower elevations along the slope and, particularly above the mountain, the geostrophic momentum constraint (A4) can be satisfied in the parameter range of Table 5. Perhaps a tentative constraint based on the present model formulation is that the parameters be restricted by Ro $\leqslant 0.3$ and $\epsilon/D \leqslant 0.5$.

REFERENCES

Blumen, W., and B. D. Gross, 1986: Semigeostrophic disturbances in a stratified shear flow over a finite-amplitude ridge. *J. Atmos. Sci.*, **43**, 3077–3088.

——, and ——, 1987: Advection of a passive scalar over a finite-amplitude ridge in a stratified rotating atmosphere. *J. Atmos. Sci.*, **44**, 1696–1705.

Davies, H. C., and K. Roth, 1986: Semi-geostrophic response of shallow water flow incident upon slender orography. I: Flow over an elongated ridge. *Ann. Geophys.*, **B4**(5), 495–506.

Gould, W. J., R. Hendry and H. E. Huppert, 1981: An abyssal topographic experiment. *Deep-Sea Res.*, **28**, 409–440.

Hoskins, B. J., 1975: The geostrophic momentum approximation and the semigeostrophic equations. *J. Atmos. Sci.*, **32**, 233–242.

Meincke, J., 1971: Observations of an anticyclonic vortex trapped above a seamount. *J. Geophys. Res.*, **76**, 7432–7440.

Merkine, L. O., and E. Kálnay-Rivas, 1976: Rotating semigeostrophic flow over finite isolated topography. *J. Atmos. Sci.*, **33**, 908–922.

Morse, P. M., and H. Feshbach, 1953: *Methods of Theoretical Physics, Part II.* McGraw-Hill, 999–1978.

Owens, W. B., and N. G. Hogg, 1980: Oceanic observations of stratified Taylor columns near a bump. *Deep-Sea Res.*, **27**, 1029–1045.

Pierrehumbert, R. T., 1985: Stratified semigeostrophic flow over two-dimensional topography in an unbounded atmosphere. *J. Atmos. Sci.*, **43**, 523–526.

Robinson, A. R., 1960: On two-dimensional flow in a rotating stratified fluid. *J. Fluid Mech.*, **9**, 321–332.

Smith, R. B., 1982: Synoptic observations and theory of orographically disturbed wind and pressure. *J. Atmos. Sci.*, **39**, 60–70.

——, 1986: Mesoscale mountain meteorology in the Alps. *Scientific Results of the Alpine Experiment, Vol. II.* GARP Publ. Ser., No. 27, WMO/TD No. 108, 407–423.